

Lunar Cratering Asymmetries with High Orbital Obliquity and Inclination of the Moon

Huacheng Li¹, Nan Zhang^{1,2}, Zongyu Yue³ and Yizhuo Zhang¹

¹ Key Laboratory of Orogenic Belts and Crustal Evolution, School of Earth and Space Sciences, Peking University, 100871 Beijing, China; nan_zhang@pku.edu.cn

² Earth Dynamics Research Group, School of Earth and Planetary Sciences, Curtin University, 6102 WA, Australia;

³ State Key Laboratory of Remote Sensing Science, Aerospace Information Research Institute, Chinese Academy of Sciences, 100101 Beijing, China; yuezy@radi.ac.cn

Received 20xx month day; accepted 20xx month day

Abstract Accurate estimation of cratering asymmetry on the Moon is crucial for understanding Moon evolution history. Early studies of cratering asymmetry have omitted the contributions of high lunar obliquity and inclination. Here, we include lunar obliquity and inclination as new controlling variables to derive the cratering rate spatial variation as a function of longitude and latitude. With examining the influence of lunar obliquity and inclination on the asteroids population encountered by the Moon, we then have derived general formulas of the cratering rate spatial variation based on the crater scaling law. Our formulas with addition of lunar obliquity and inclination can reproduce the lunar cratering rate asymmetry at the current Earth-Moon distance and predict the apex/ant-apex ratio and the pole/equator ratio of this lunar cratering rate to be 1.36 and 0.87, respectively. The apex/ant-apex ratio is decreasing as the obliquity and inclination increasing. Combining with the evolution of lunar obliquity and inclination, our model shows that the apex/ant-apex ratio does not monotonically decrease with Earth-Moon distance and hence the influences of obliquity and inclination are not negligible on evolution of apex/ant-apex ratio. This model is generalizable to other planets and moons, especially for different spin-orbit resonances.

Key words: Moon, meteorites, meteors, meteoroids, planets and satellites: surfaces

1 INTRODUCTION

Cratering asymmetry on the lunar surface has been recognized in many studies (Le Feuvre & Wieczorek 2011; Wang & Zhou 2016). Understanding of such asymmetry alters the basis of lunar cratering chronology (Hiesinger et al. 2000; Fassett et al. 2012), because it has assumed cratering rate is spatially uniform

on the whole Moon (McGill 1977), which eventually influences the fundamental understanding of lunar evolution. Quantifying the asymmetry can rectify the deviation in counting the lunar craters sampled by Apollo and Luna missions (Hartmann 1970; Neukum et al. 1975; Neukum 1984). Cratering asymmetry has been also generalized to the surface datings of other planets or moons (Horedt & Neukum 1984; Neukum et al. 2001a,b; Hartmann & Neukum 2001; Zahnle et al. 2001; Korycansky & Zahnle 2005). Various factors affecting the cratering asymmetry on the Moon have been intensively investigated (Hartmann 1970; Neukum et al. 1975; Neukum 1984; Le Feuvre & Wieczorek 2011; Wang & Zhou 2016), and the key factors affecting the cratering asymmetry include (1) the speed and inclination of asteroids encountering the Moon (Le Feuvre & Wieczorek 2011) and (2) the distance between the Earth and the Moon (Zahnle et al. 2001; Le Feuvre & Wieczorek 2011; Wang & Zhou 2016).

Three types of cratering asymmetries, i.e., the leading/trailing asymmetry, pole/equator asymmetry, and near/far-side asymmetry have been recognized (e.g., Le Feuvre & Wieczorek 2011; Wang & Zhou 2016). The leading/trailing asymmetry has been explained by both theoretic derivations (Horedt & Neukum 1984; Le Feuvre & Wieczorek 2011; Wang & Zhou 2016) and numerical simulations (Gallant et al. 2009; Wang & Zhou 2016). It has been confirmed that the leading surface receives more impactor fluxes and higher impact speed than the trailing surface due to the synchronous rotating, while this difference declines with the Earth-Moon distance increased (Le Feuvre & Wieczorek 2011; Wang & Zhou 2016). The pole/equator asymmetry has also been numerically modelled (Gallant et al. 2009; Wang & Zhou 2016), which suggested that low latitude of the Moon receives more impactor fluxes for the gathering of low inclination asteroids (Le Feuvre & Wieczorek 2008, 2011). In addition, the pole/equator asymmetry is found to vary by less than %1 when the Earth-Moon distance is between 20 and 60 Earth radii (Le Feuvre & Wieczorek 2011). The mechanism of near/far-side asymmetry has not reached a consensus (Wiesel 1971; Bandermann & Singer 1973). In previous studies, two factors affecting impact asymmetry, i.e., orbital obliquity and inclination of the Moon (relative to the ecliptic), have been usually neglected (Le Feuvre & Wieczorek 2011; Wang & Zhou 2016). However, these two factors might be important within the first 35 Earth radii of Earth-Moon distance when the Moon quickly left Earth (Ćuk et al. 2016; Ward 1975). Therefore, it is necessary to investigate the influences of these two factors on the lunar cratering asymmetries.

In this study, we derive the impact asymmetry reliance on the orbital obliquity and inclination of the Moon by improving previous empirical models of leading/trailing and pole/equator asymmetries (Le Feuvre & Wieczorek 2011) and extending two-dimensional analytic formulas (Wang & Zhou 2016) to the complete formulas based on three-dimensional geometry. Le Feuvre & Wieczorek (2011) assumed the orbital obliquity of the Moon was constant when the Earth-Moon distance is larger than 20 Earth radii. Wang & Zhou (2016) calculated the cratering asymmetries in a planar model which excludes the influences of the orbital obliquity and inclination of the Moon. Our analytical formulation including obliquity and inclination can reveal more features of lunar leading/trailing asymmetry (Le Feuvre & Wieczorek 2011) and add explicit term for the pole/equator asymmetry (Wang & Zhou 2016). In Section 2, we derived the formulas for the distribution of impact flux, normal speed, and cratering rate on the Moon using the concentration of asteroids encountering with the Moon and scaling laws that convert asteroids velocities and diameters to the diameters of craters (Holsapple & Housen 2007). Section 3 shows the resultant distributions of impact

Table 1: Variables or Parameters Used in the Method.

Description	Notation	Range
inclination of asteroids' encounter velocity	ϕ_p	$[-\frac{\pi}{2}, \frac{\pi}{2}]$
azimuth of asteroids' encounter velocity	λ_p	$[0, 2\pi]$
encounter speed of asteroids	v_p	$[19km/s, \sim 20km/s]$
lunar orbit inclination	i_1	$[0, \frac{\pi}{2}]$
lunar obliquity relative to the ecliptic	i_2	$[0, \frac{\pi}{2}]$
azimuth of lunar orbit normal	ω_1	$[0, 2\pi]$
azimuth of lunar spin axis	ω_2	$[0, 2\pi]$
lunar true anomaly	f_m	$[0, 2\pi]$
lunar eccentric anomaly	E	$[0, 2\pi]$
lunar mean anomaly	M	$[0, 2\pi]$
lunar argument of perihelion	ω_3	$[0, 2\pi]$
longitude of impact sites	λ	$[0, 2\pi]$
latitude of impact sites	ϕ	$[-\frac{\pi}{2}, \frac{\pi}{2}]$
semi-major axis of lunar orbit	a_m	$[25R_e, 60R_e]$
eccentricity of lunar orbit	e	$[0, 1)$

flux, normal speed, and cratering rate based on formulas in Section 2. This result section also estimates the evolution of the apex/ant-apex ratio of cratering rate according to the evolution of orbital obliquity and inclination with different Earth-Moon distances (Ćuk et al. 2016). In Section 4, we verify formulas in Section 2 by comparing with previous results and explain how the orbital obliquity and inclination influence the lunar cratering rate asymmetry. Additionally, the influences of orbital obliquity and inclination of the Moon on the concentration of asteroids encountering with the Moon are detailed in the appendix.

2 METHOD

This section shows how we calculate the distribution of asteroids impact flux, impact speed and cratering rate using variables in Table 1. Section 2.1 introduces assumptions and coordinate systems with which we derive the expression of asteroid's velocity \vec{v}_p and the normal vector \vec{n} at the impact site. \vec{v}_p and \vec{n} will be used in the following calculations. Section 2.2 uses equations from Wang & Zhou (2016) and Le Feuvre & Wieczorek (2011) to estimate the impact flux at different impact sites. These equations are rewritten as functions of \vec{v}_p and \vec{n} . Section 2.3 calculates the cratering rate variation using scaling law from Holsapple & Housen (2007). Obtaining the cratering rate variation requires the impact flux variation and impact normal speed variation. The former has been calculated in section 2.2 and the later can be calculated with minor changes in calculation of impact flux.

2.1 Asteroids Velocity and Normal Vector at Impact Site

This model assumes the orbit of the Moon is an ellipse with the Earth as a focus. Then in the geocentric ecliptic coordinate system (Z-axis is parallel to the ecliptic normal and X-axis is towards mean equinox of the J2000 epoch), the position and velocity of the Moon are \vec{r}_m and \vec{v}_m . We note that the influence of variation of i_1, ω_1 or ω_3 on the lunar velocity can be estimated using Eqs. (2-5) of Ćuk & Burns (2004) and

is $< 1\%$ compared to the influence of variation of f_m . We hence ignored the variation of i_1, ω_1 or ω_3 in deriving the lunar velocity. In Eq. (2), G and M_e are the gravitational constant and the mass of the Earth respectively.

$$\vec{r}_m = R_z\left(\frac{\pi}{2} + \omega_1\right)R_x(i_1)R_z(\omega_3)\vec{r} \quad (1)$$

$$\vec{r} = \left[\frac{a_m(1-e^2)}{1+e\cos f_m} \cos f_m, \frac{a_m(1-e^2)}{1+e\cos f_m} \sin f_m, 0 \right]^T$$

$$\vec{v}_m = R_z\left(\frac{\pi}{2} + \omega_1\right)R_x(i_1)R_z(\omega_3)\vec{v} \quad (2)$$

$$\vec{v} = \left[-\sqrt{\frac{GM_e}{a_m(1-e^2)}} \sin f_m, \sqrt{\frac{GM_e}{a_m(1-e^2)}} (e + \cos f_m), 0 \right]^T$$

$$R_x(\theta) = \begin{bmatrix} 1 & 0 & 0 \\ 0 & \cos \theta & -\sin \theta \\ 0 & \sin \theta & \cos \theta \end{bmatrix}, \quad R_z(\theta) = \begin{bmatrix} \cos \theta & -\sin \theta & 0 \\ \sin \theta & \cos \theta & 0 \\ 0 & 0 & 1 \end{bmatrix}$$

The population concentration C_0 of asteroids encountering with the Moon is defined as the distribution of the relative number of asteroids that encounter with the Moon within a unit time and it can be determined by their velocities (e.g., Figure 5 of Le Feuvre & Wieczorek 2008). In Eq. (3) and (4), \vec{v}_p and \vec{e}_z are the asteroids' encounter velocity in the geocentric ecliptic coordinate system and an unit vector parallel to the positive Z-axis respectively. v_p is the average encounter velocity of the asteroids related to the Earth.

$$C_0 = p(\vec{v}_p) = p(\lambda_p, \phi_p) \quad (3)$$

$$\vec{v}_p = v_p R_z\left(\frac{\pi}{2} + \lambda_p\right)R_x\left(\frac{\pi}{2} - \phi_p\right)\vec{e}_z \quad (4)$$

In this model, \vec{v}_p is determined by λ_p, ϕ_p , and v_p . The concentration of asteroids encountering with the Moon is assumed unaffected by the orbital obliquity and inclination of the Moon (see the appendix A). Eq. (A.20) indicates the concentration of asteroids encountering with the Moon can be estimated by the concentration encountering with the Earth. Then C_0 should be function of (v_p, λ_p, ϕ_p) . Spectrum of v_p is not considered in this study and it is set as the average encounter speed (Horedt & Neukum 1984; Zahnle et al. 2001). Then C_0 is independent of v_p and a function of (λ_p, ϕ_p) . Since the precession of lunar orbit, the asteroids' azimuth distribution will not affect the cratering asymmetries. Therefore, only the marginal distribution of Eq. (3) $\int_{-\pi}^{\pi} C_0 d\lambda_p$ is required in the calculation of cratering asymmetries. This marginal distribution is taken from Le Feuvre & Wieczorek (2008) and it has been shown in Figure 6 of Le Feuvre & Wieczorek (2008).

The Moon is assumed to be synchronously rotating with a constant angular velocity and the prime meridian is determined by the mean sub-Earth point (GSFC 2008). In the lunar fixed coordinate system whose X-axis is the intersection of the lunar equator plane and prime meridian plane, and Z-axis is the lunar spin axis, the normal at lunar surface is $\vec{n}(\lambda, \phi)$ and the transformation matrix T from this lunar fixed coordinate system to the geocentric ecliptic coordinate system are determined by ω_2, i_2 and M . The relationship between coordinate systems used in this section is illustrated in Figure 1.

$$\vec{n}(\lambda, \phi) = R_z\left(\frac{\pi}{2} + \lambda\right)R_x\left(\frac{\pi}{2} - \phi\right)\vec{e}_z \quad (5)$$

$$T = R_z\left(\frac{\pi}{2} + \omega_2\right)R_x(i_2)R_z(M + M_0) \quad (6)$$

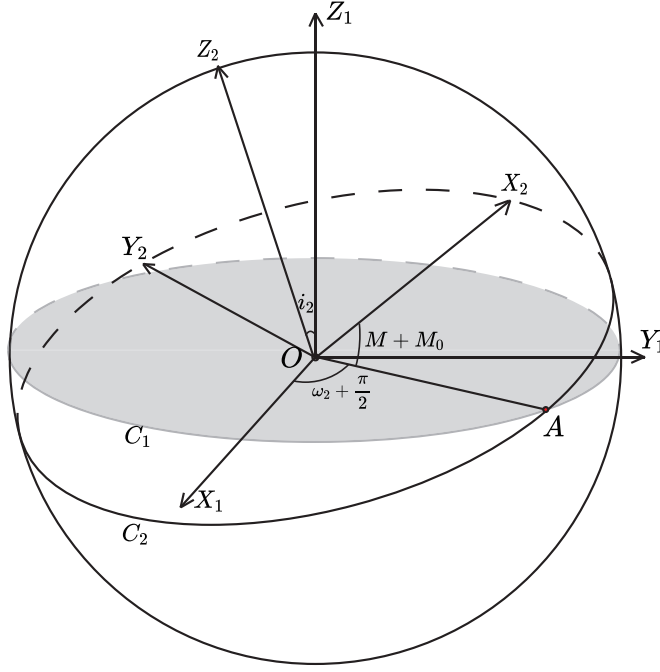


Fig. 1: The coordinate systems used in calculation. The geocentric ecliptic coordinate system is $OX_1Y_1Z_1$. The lunar fixed coordinate system is $OX_2Y_2Z_2$ and its origin is translated to the Earth. The gray plane C_1 is the ecliptic plane. The plane C_2 is the lunar equatorial plane. \overline{OA} is the intersection of C_1 and C_2 .

In Eq. (6), M_0 is a parameter related to the position of the mean sub-Earth point and it will be determined by Eqs. (7-9). When the Moon at the perigee, the center of Earth passes through the lunar prime meridian plane.

$$\left. \frac{r_m}{|r_m|} \right|_{f_m=0} + T \cdot \vec{n}(0, \phi) = 0 \quad (7)$$

Solving Eq. (7), this gives

$$\cos M_0 = \frac{\cos i_1 \sin(\omega_1 - \omega_2) \sin \omega_3 - \cos(\omega_1 - \omega_2) \cos \omega_3}{\sqrt{1 - (\sin i_2 \sin(\omega_1 - \omega_2) \cos \omega_3 - \cos i_1 \sin i_2 \cos(\omega_1 - \omega_2) \sin \omega_3 - \sin i_1 \cos i_2 \sin \omega_3)^2}} \quad (8)$$

$$\sin M_0 = \frac{-\cos i_1 \cos i_2 \cos(\omega_1 - \omega_2) \sin \omega_3 - \cos i_2 \sin(\omega_1 - \omega_2) \cos \omega_3 + \sin i_1 \sin i_2 \sin \omega_3}{\sqrt{1 - (\sin i_2 \sin(\omega_1 - \omega_2) \cos \omega_3 - \cos i_1 \sin i_2 \cos(\omega_1 - \omega_2) \sin \omega_3 - \sin i_1 \cos i_2 \sin \omega_3)^2}} \quad (9)$$

2.2 Distribution of Impact Flux

For given \vec{v}_p , r_m and \vec{v}_m , the velocity of asteroids relative to the Moon is $\vec{v}_p - \vec{v}_m$. Define \hat{x} as $\frac{\vec{v}_p - \vec{v}_m}{|\vec{v}_p - \vec{v}_m|}$. ($T\vec{n}(\lambda, \phi)$). The impact flux δF is defined as the distribution of the number of asteroids that impact on the lunar surface within a unit area and a unit time. According to Eq. (26) of Wang & Zhou (2016) and Eq. (A.47) of Le Feuvre & Wieczorek (2011), the impact flux δF is a function of \hat{x} . In Eq. (13), M_m and R_m

are the mass and radius of the Moon respectively.

$$\delta F = C_0 |v_p^{\vec{}} - v_m^{\vec{}}| f(\hat{x}) \quad (10)$$

$$f_1(\hat{x}) = \begin{cases} \hat{x} & , \hat{x} \geq 0 \\ 0 & , \hat{x} < 0 \end{cases} \quad (11)$$

$$f_2(x) = \begin{cases} \frac{1}{4}(1 + \Gamma)^{-1}(1 + \mu^{-1})(\Gamma + (1 + \mu)\hat{x}) & , \hat{x} \geq \frac{-\Gamma}{2 + \Gamma} \\ 0 & , \hat{x} < \frac{-\Gamma}{2 + \Gamma} \end{cases} \quad (12)$$

$$\mu = \sqrt{1 + \frac{2\Gamma}{1 + \hat{x}}}, \Gamma = \frac{2GM_m}{|v_p^{\vec{}} - v_m^{\vec{}}|^2 R_m} \quad (13)$$

where $f_1(\hat{x})$ and $f_2(\hat{x})$ are two forms of $f(\hat{x})$. $f_1(\hat{x})$ is from Wang & Zhou (2016) which assumes the trajectories of asteroids are straight lines in the direction of their common encounter velocity. While $f_2(\hat{x})$ is from Le Feuvre & Wieczorek (2011) in which trajectories of asteroids are treated as hyperbolic curve with a focus at the center of the Moon. Because $\Gamma < 0.02$, we can expand Eq. (12) around 0 with Taylor series.

$$f_2(\hat{x}) = \hat{x} + \left(\frac{1}{2} - 2\hat{x}\right)\Gamma + \frac{4\hat{x}^3 + 6\hat{x}^2 - 3}{4(1 + \hat{x})^2}\Gamma^2 + o(\Gamma^3) \quad \hat{x} > \frac{-\Gamma}{2 + \Gamma} \quad (14)$$

Obviously, $f_1(\hat{x})$ is the first order approximation of $f_2(\hat{x})$. The absolute relative difference between f_1 and f_2 is less than %3.5. For simplicity, we use $f(\hat{x}) = f_1(\hat{x})$ in following calculations. Then the average flux within a period of lunar orbit is

$$F = \frac{1}{2\pi} \int_0^{2\pi} \delta F dM = \frac{1}{2\pi} \int_0^{2\pi} C_0 |v_p^{\vec{}} - v_m^{\vec{}}| f(\hat{x}) dM \quad (15)$$

It is known today that ω_3 changes with a period of 8.85 years and ω_2 changes with a period of 18.61 years. The secular average flux independent of them is

$$\bar{F}(\lambda, \phi; a_m, e, i_1, i_2, v_p) = \int_0^{2\pi} \frac{d\omega_3}{2\pi} \int_0^{2\pi} \frac{d\omega_2}{2\pi} \int_0^{2\pi} \frac{d\lambda_p}{2\pi} \int_{-\frac{\pi}{2}}^{\frac{\pi}{2}} F \frac{d\phi_p}{\pi} \quad (16)$$

2.3 Distribution of Normal Impact Speed and Cratering Rate

In this model, the impact angle of asteroids at lunar surface is θ (Eq. (A.54) of Le Feuvre & Wieczorek 2011) and the normal impact speed is V_{\perp} (Eqs. (A.50-A.51) of Le Feuvre & Wieczorek 2011).

$$V_{\perp} = |v_p^{\vec{}} - v_m^{\vec{}}| \sqrt{1 + \Gamma} \sin \theta = |v_p^{\vec{}} - v_m^{\vec{}}| g(\hat{x}) \quad (17)$$

$g(\hat{x})$ can also be written as two different forms $g_1(\hat{x})$ and $g_2(\hat{x})$. $g_1(\hat{x})$ is from Wang & Zhou (2016) and $g_2(\hat{x})$ is from Le Feuvre & Wieczorek (2011).

$$g_1(\hat{x}) = \hat{x} / \sqrt{1 + \Gamma} \quad (18)$$

$$\begin{aligned} g_2(\hat{x}) &= \sqrt{1 + \Gamma - \left(\frac{1 + \mu}{2}\right)^2 (1 - \hat{x}^2)} \\ &= |\hat{x}| + \frac{1}{2} \text{sgn}(\hat{x}) \Gamma - \frac{\text{sgn}(\hat{x})}{4(1 + \hat{x})} \Gamma^2 + o(\Gamma^3) \end{aligned} \quad (19)$$

Similar to $f(\hat{x})$, we expand $g_2(\hat{x})$ around $\Gamma = 0$. $g_1(\hat{x})$ is the first order approximation of $g_2(\hat{x})$. Substituting $g_1(\hat{x})$ in to Eq. (17). We obtain the average normal speed

$$\bar{V}_\perp(\lambda, \phi; a_m, e, i_1, i_2, v_p) = \frac{1}{\bar{F}(\lambda, \phi; a_m, e, i_1, i_2, v_p)} \int_0^{2\pi} \frac{d\omega_3}{2\pi} \int_0^{2\pi} \frac{d\omega_2}{2\pi} \int_0^{2\pi} \frac{d\lambda_p}{2\pi} \int_{-\frac{\pi}{2}}^{\frac{\pi}{2}} \frac{d\phi_p}{\pi} \int_0^{2\pi} \delta F V_\perp \frac{dM}{2\pi} \quad (20)$$

Combing Eq. (16) and Eq. (20), we finally obtain the cratering rate expression. Similar to Eq. (56) of Wang & Zhou (2016) and applying the scaling law of crater diameters(e.g., Holsapple & Housen (2007)), the cratering rate in our model is

$$N_c(\lambda, \phi; a_m, e, i_1, i_2, v_p) \propto (\bar{V}_\perp(\lambda, \phi; a_m, e, i_1, i_2, v_p))^{\gamma_p \alpha_p} \bar{F}(\lambda, \phi; a_m, e, i_1, i_2, v_p) \quad (21)$$

Here the cratering rate calculation only takes account the the near-Earth objects: $\gamma_p \alpha_p = 0.987$ (Bottke et al. 2002; Holsapple & Housen 2007). α_p is an exponent in the cumulative size distribution of near-Earth objects diameter (Bottke et al. 2002). γ_p is a parameter in the scaling law (Holsapple & Housen 2007; Le Feuvre & Wieczorek 2011; Wang & Zhou 2016).

3 RESULT

In this section, we describe the cratering rate asymmetry produced by Eq. (21). Section 3.1 demonstrates the spatial variation of impact flux, normal speed, and cratering rate. Section 3.2 reveals the influences of orbital obliquity and inclination of the Moon on lunar cratering rate asymmetry. Section 3.3 provides the evolution of apex/ant-apex ratio with orbital obliquity and inclination of the Moon.

3.1 Spatial Variations of Impact Flux, Normal Speed, and Cratering Rate

First, our derived formula is used to calculate the cratering rate spatial variation at current values of the Earth-Moon system since such variation can be compared with previous predictions by Le Feuvre & Wieczorek (2011) and Wang & Zhou (2016). Figure 2 shows the relative spatial variation of impact flux, normal speed, and cratering rate on the Moon with parameters set at current values of the Earth-Moon system. The parameters involved in Eq. (21) are set as $(a_m, e, i_1, i_2, v_p) = (60R_e, 0.0549, 5.145^\circ, 1.535^\circ, 19km/s)$ (R_e is the radius of the Earth). In Figure 2, the relative cratering rate is symmetry about $0^\circ N$. This symmetry arises from the symmetry of the asteroids's concentration C_0 . The maximum of impact flux occurs at $(90^\circ W, 0^\circ N)$ and the minimum is at $(90^\circ E, \pm 65^\circ N)$. The maximum/minimum ratio of impact flux is 1.24. The maximum of normal speed occurs at $(90^\circ W, 0^\circ N)$ and the minimum is at $(90^\circ E, \pm 47^\circ N)$. The maximum normal speed is $13.7 km/s$ and the minimum is $12.1 km/s$. The maximum of cratering rate occurs at $(90^\circ W, 0^\circ N)$ and the minimum is at $(90^\circ E, \pm 53^\circ N)$. The maximum/minimum cratering rate ratio is 1.40. The apex/ant-apex ratio (the cratering rate ratio between $(90^\circ W, 0^\circ N)$ and $(90^\circ E, 0^\circ N)$) is 1.36 and this ratio is a measure of the longitudinal variation. The pole/equator ratio is 0.87 and this is a measure of the latitudinal variation. The impact flux, normal speed, and cratering rate with $e = 0$ (other parameters are set same as Figure 2) are also calculated. The relative difference of cratering rate ($e = 0$) from Figure 2 is less than 0.2%.

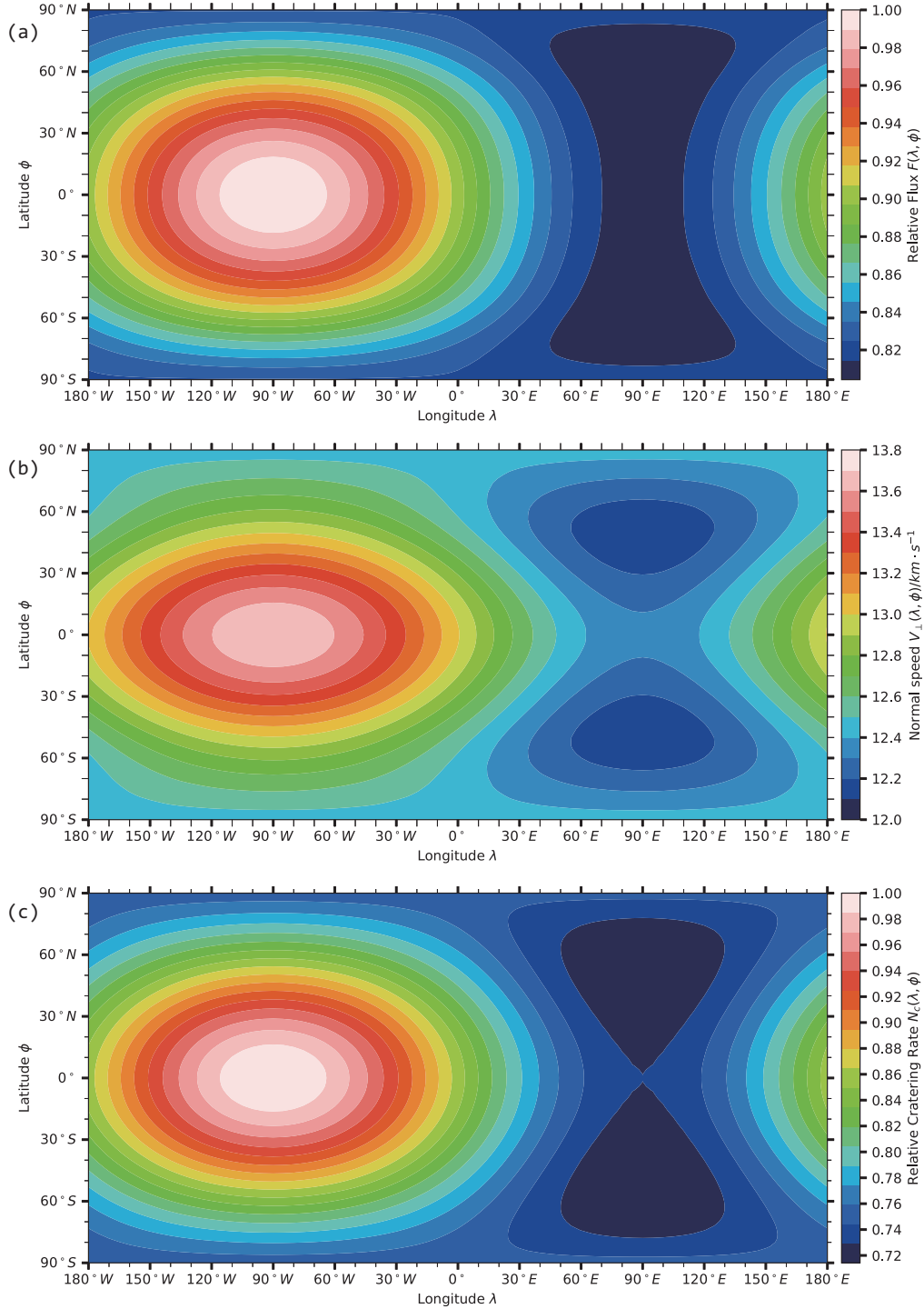


Fig. 2: Distribution of impact flux (a), normal speed (b), and cratering rate (c) on the Moon for the current lunar orbital obliquity, inclination and Earth-Moon distance. The maximum is set to 1.00.

3.2 Influences of Orbital Inclination and Obliquity of the Moon

We next investigate the specific effects of lunar orbital inclination and obliquity on apex/ant-apex and pole/equator ratios. Figure 3 shows the apex/ant-apex ratio r_1 and pole/equator ratio r_2 with different lunar inclination and obliquity. i_2 is not same with the lunar obliquity to its orbit normal. For Cassini state

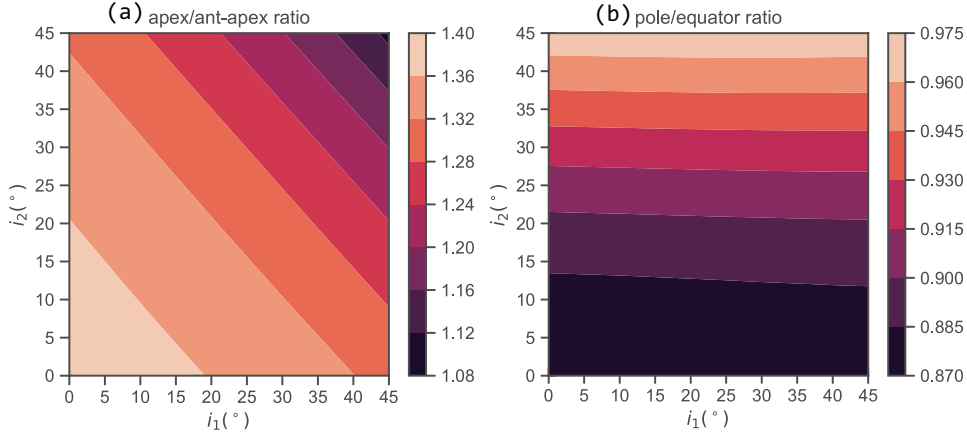


Fig. 3: The apex/ant-apex (a) and pole/equator (b) ratios with orbital obliquity and inclination of the Moon. Only the Cassini state 2 ($\omega_1 = \omega_2 + \pi$) is calculated.

2 ($\omega_1 = \omega_2 + \pi$), lunar obliquity relative to the lunar orbit normal is $i_1 + i_2$, while for Cassini state 1 ($\omega_1 = \omega_2$), lunar obliquity relative to the lunar orbit normal is $|i_1 - i_2|$ (Ward 1975). Other parameters in Eq. (21) are set as $(a_m, e, v_p) = (60R_e, 0.0549, 19\text{km/s})$. r_1 decreases with both i_1 and i_2 increased, while r_2 increases with increase in i_2 and seems to be independent of i_1 . Based on our calculated i_1 and i_2 distribution, we speculate the correlation of r_1 or r_2 with $\cos(i_1 + i_2)$ and $\cos(2i_2)$ can be fitted as linear regressions.

$$r_1 = a_{11} + a_{12} \cos(i_1 + i_2) + a_{13} \cos(2i_2) \quad (22)$$

$$r_2 = a_{21} + a_{22} \cos(i_1 + i_2) + a_{23} \cos(2i_2) \quad (23)$$

When $a_m = 60R_e$, the fitting result is

$$\begin{pmatrix} a_{11} & a_{12} & a_{13} \\ a_{21} & a_{22} & a_{23} \end{pmatrix} = \begin{pmatrix} 1.12676 & 0.2469790 & 0.0089461 \\ 0.97137 & -0.0029778 & -0.0930123 \end{pmatrix} \quad (24)$$

When i_1 and i_2 are between 0° and 45° , the relative error between fitting result and Figure 3 is less than 2.4% for r_1 and 0.15% for r_2 .

3.3 Evolution of the Apex/ant-apex Ratio

The past obliquity has been very high and the lunar inclination is also different from current value (Ward 1975; Ćuk et al. 2016). We obtain the evolution of the lunar orbital obliquity and inclination with the Earth-Moon distance by reproducing the semi-analytical method for the lunar orbital evolution from Ćuk et al. (2016). This method includes solving the differential equations of lunar synchronous orbit controlled by Earth and Moon tidal dissipation, as well as coupling them with the equation to satisfy the Cassini state Ward (1975). The solutions show that the lunar inclination damps from the initial high value to its present low value 5.1° due to tidal dissipation, and the lunar obliquity first increases and then decreases to current value 1.5° with the jump between $29.7R_e$ and $35R_e$ due to the transitions from Cassini state 1 to Cassini state 2, which is similar to the extended data Figure 1 in Ćuk et al. (2016). We next apply this evolution in our model to estimate the evolution of apex/ant-apex ratio (Figure 4). According to Ćuk et al. (2016), the

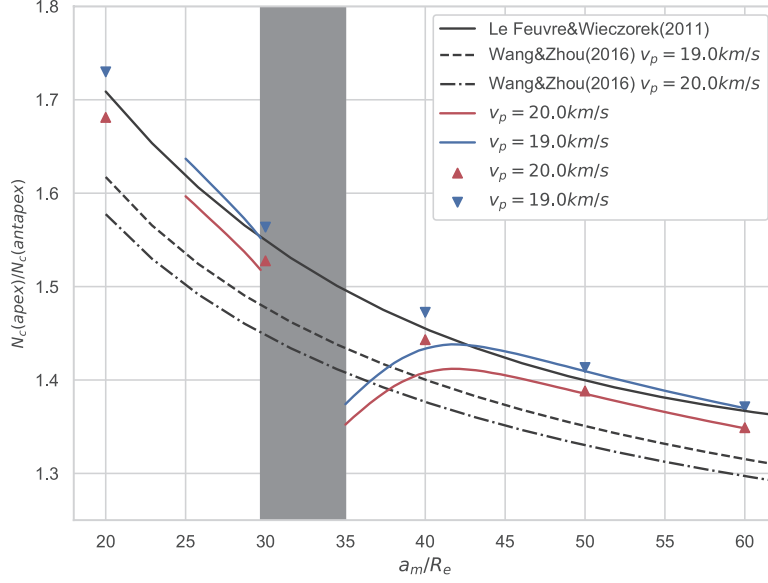


Fig. 4: Evolution of the apex/ant-apex ratio with Earth-Moon distance. The X-axis represents the Earth-Moon distance and Y-axis represents the apex/ant-apex ratio. The black solid line is $1.12e^{-0.0529a_m/R_e} + 1.32$ from Le Feuvre & Wieczorek (2011). The value of $\alpha_p \gamma_p$ in Le Feuvre & Wieczorek (2011) ranges from 0.907 to 1.25. The other two dashed black curves represent Eq. (124) of Wang & Zhou (2016) with $\alpha_p \gamma_p = 0.987$. The red and blue triangles represent results from Eq. (21) which uses constant obliquity and inclination same as current values $(i_1, i_2) = (5.145^\circ, 1.535^\circ)$. The red and blue lines is calculated basing on the evolution of orbital obliquity and inclination of the Moon from Ćuk et al. (2016) with lunar tidal dissipation number $Q_M = 38$.

Moon is in non-synchronous rotation from $29.7R_e$ to about $35R_e$ (gray box in Figure 4). When the Moon is at Cassini state 1 (the Earth-Moon distance $< 29.7R_e$), the apex/ant-apex ratio decreases with a_m . When the Moon is at Cassini state 2 ($> 35R_e$), this ratio reaches a maximum between $40R_e$ and $45R_e$.

3.4 Cratering Rate Distribution of 3:2 Resonance

Our formulas can also predict cratering rate distributions with various spin-orbit resonance. When the resonance is 3:2 (applicable to Mercury, Colombo 1965), we have a different transformation matrix in Eq. (6) as

$$T' = R_z\left(\frac{\pi}{2} + \omega_2\right)R_x(i_2)R_z\left(\frac{3}{2}M + M_0\right) \quad (25)$$

Also because this resonance is 3:2, a full integration interval for Eqs. (16), (20), and (21) is extended to two periods $(0, 4\pi]$. If setting up the parameters involved in Eq. (21) as those for Mercury $(\sqrt{GM_e/a_m}, e, i_1, i_2, v_p) = (48.0 \text{ km/s}, 0.205, 7.0^\circ, 7.0^\circ, 42.2 \text{ km/s})$. Further substituting T in Eqs. (7-21) with T' and using the asteroids inclination distribution from Le Feuvre & Wieczorek (2008), the maximum and minimum of cratering rate with 3:2 resonance is at $(\pm 90^\circ E, 0^\circ N)$ and $\pm 90^\circ N$, respectively. The maximum/minimum cratering rate ratio is 3.64. When the orbital eccentric is degraded to 0.0 (Le Feuvre &

Wieczorek 2008; Wang & Zhou 2016), the maximum and minimum are at $0^\circ N$ and $\pm 90^\circ N$, respectively. The maximum/minimum cratering rate ratio is 2.91.

4 DISCUSSION

4.1 Comparison with Previous Results

In Figure 2(c), this study gives a similar current cratering rate spatial variation ($a_m = 60R_e$) as Le Feuvre & Wieczorek (2011) in which the maximum and minimum appear at $(90^\circ W, 0^\circ N)$ and $(90^\circ E, \pm 65^\circ N)$ respectively. The difference in the location of the minimum between our result and Le Feuvre & Wieczorek (2011) may be brought by f_1 and g_1 used in our calculations. The apex/ant-apex ratio for current Moon from Le Feuvre & Wieczorek (2011) is 1.37. The apex/ant-apex ratio for current Moon from Wang & Zhou (2016) with $v_p = 19 \text{ km/s}$, $\alpha_p \gamma_p = 0.987$ and this study are 1.32 and 1.36 respectively. As an extension based on Le Feuvre & Wieczorek (2011) and Wang & Zhou (2016), this study gives a value between them. The larger relative difference between this study and Wang & Zhou (2016) is probably caused by either the asteroids inclination or the orbital obliquity and inclination of the Moon. The pole/equator ratio in Figure 2(c) is 0.87. This value is higher than 0.80 in Le Feuvre & Wieczorek (2011). This difference may be brought by f_1 and g_1 used in our calculations. Besides the current cratering rate, this study also gives the evolution of the apex/ant-apex ratio in Figure 4. The results from Le Feuvre & Wieczorek (2011) and Wang & Zhou (2016) are also included in Figure 4. The value of $\alpha_p \gamma_p$ adopted in Le Feuvre & Wieczorek (2011) is about $0.907 \sim 1.25$, because they used different parameters in crater scaling law (in non-porous gravity scaling regime $\gamma_p = 0.564$ while in porous $\gamma_p = 0.410$) and a 10th-order polynomial to fit the size distribution of asteroids ($\alpha_p \approx 2.22$). The influences of $\alpha_p \gamma_p$ is shown in Figure 5. When $\alpha_p \gamma_p$ is between $0.907 \sim 1.25$ and v_p is between $19 \sim 20 \text{ km/s}$, the apex/ant-apex ratio for current Moon calculated by this model is about $1.33 \sim 1.41$. Although the value of $\alpha_p \gamma_p$ or v_p in this study is different from Le Feuvre & Wieczorek (2011), if the orbital obliquity and inclination of the Moon is assumed constant and same with current values $(i_1, i_2) = (5.145^\circ, 1.535^\circ)$, this study will reproduce the results predicted by Le Feuvre & Wieczorek (2011) (red and blue triangle in Figure 4).

If we consider the variation of obliquity and inclination, when the Earth-Moon distance is more than $\sim 42R_e$, this model gives a consistent value with Le Feuvre & Wieczorek (2011) and a similar trend with Wang & Zhou (2016). However, when Earth-Moon distance is between $35R_e$ and $\sim 42R_e$, this study gives an opposite trend to previous results. According to Čuk et al. (2016), the orbital obliquity and inclination of the Moon decrease in this interval. This evolution trend of apex/ant-apex ratio can be explained by the influences of orbital obliquity and inclination of the Moon. When Earth-Moon distance is between $29.7R_e$ and $35R_e$, the Moon is in non-synchronous rotation and the apex/ant-apex ratio will be diminished by non-synchronous rotation. When Earth-Moon distance is less than $29.7R_e$, the apex/ant-apex ratio is calculated under the assumption: the inclination distribution of asteroids' velocity is same as current distribution. Although the obliquity and inclination is very high, the apex/ant-apex ratio is consistent with Le Feuvre & Wieczorek (2011). We note that the population of asteroids is dominated by main-belt asteroids during the late heavy bombardment and near-Earth objects since $3.8 - 3.7 \text{ Ga}$ according to Strom et al. (2015). The population of near-Earth objects have been in steady state for the past $\sim 3 \text{ Ga}$ (Bottke et al. 2002). The

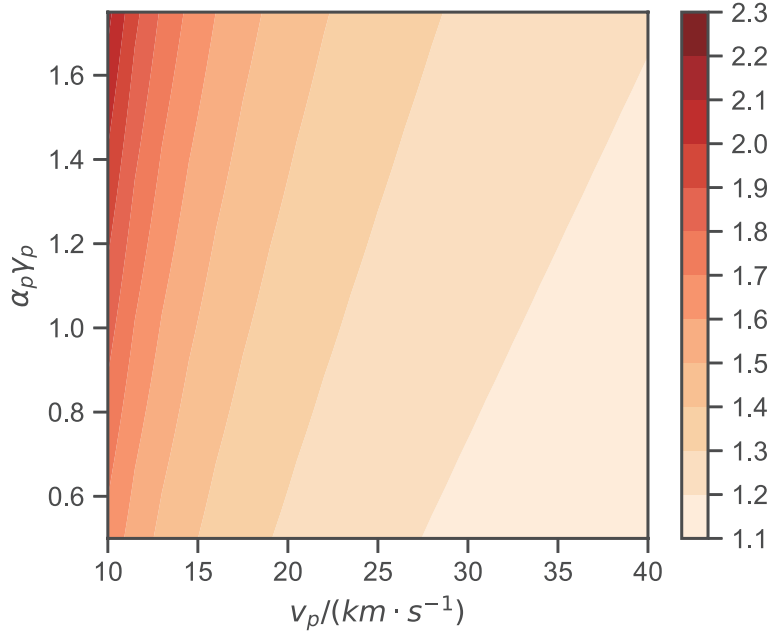


Fig. 5: Apex/ant-apex ratio of cratering rate with different $\alpha_p \gamma_p$ and v_p . Other parameters involved in Eq. (21) is set as $(a_m, e, i_1, i_2) = (60R_e, 0.0549, 5.145^\circ, 1.535^\circ)$.

evolution of apex/ant-apex ratio for the Earth-Moon distance $< 29.7R_e$ may be quite different from that shown in Figure 4. It is confirmed that the influences of orbital obliquity and inclination of the Moon are not negligible in analysing lunar cratering asymmetry.

4.2 Explanation for the Influences of Orbital Obliquity and Inclination of the Moon

When the lunar orbit eccentric $e = 0.0$, our model is sketched in Figure 6. In a lunar rotation period, the relative position between $\{\vec{n}, \vec{k}, \vec{s}\}$ and the coordinate system $OX_2Y_2Z_2$ is not fixed. The apex or ant-apex point is on the gray cycle C_2 . When $i_1 = i_2 = 0$, the gray circle C_2 , red circle, and yellow circle coincide and r_1 reaches its maximum. The influence of asteroids inclination is related to the length of \widehat{AC} . The influence of lunar velocity is related to the length of \widehat{AB} . The farther the ant-apex is from B or C , the smaller the leading/trailing asymmetry. In our model, the angular distance between A (ant-apex) and B is in $[0, \max\{|i_1 + i_2|, |i_1 - i_2|\}]$ and the angular distance between A and C is in $[0, i_2]$. For Cassini state 2, $\max\{|i_1 + i_2|, |i_1 - i_2|\} = |i_1 + i_2|$. This is consistent with the fitting result: r_1 is proportional to $\cos(i_1 + i_2)$ and $\cos(2i_2)$. For r_2 which is related to the angular distance between point D and the red or yellow plane. When $i_1 = i_2 = 0$, r_2 reaches its minimum. The angular distance between point D and the red circle is in $[0, i_2]$ and the angular distance between point D and the yellow circle is in $[0, \max\{|i_1 + i_2|, |i_1 - i_2|\}]$. The pole/equator asymmetry will decrease with increasing in those two angular distances. This is also consistent with the fitting result: r_2 is proportional to $\cos(2i_2)$ and $\cos(i_1 + i_2)$.

4.3 Generalization of this Model

The orbital obliquity and inclination of the Moon, Earth-Moon distance, lunar orbital eccentric, and lunar rotation speed have been included in this model. In addition to the Moon, this model can be applied to other

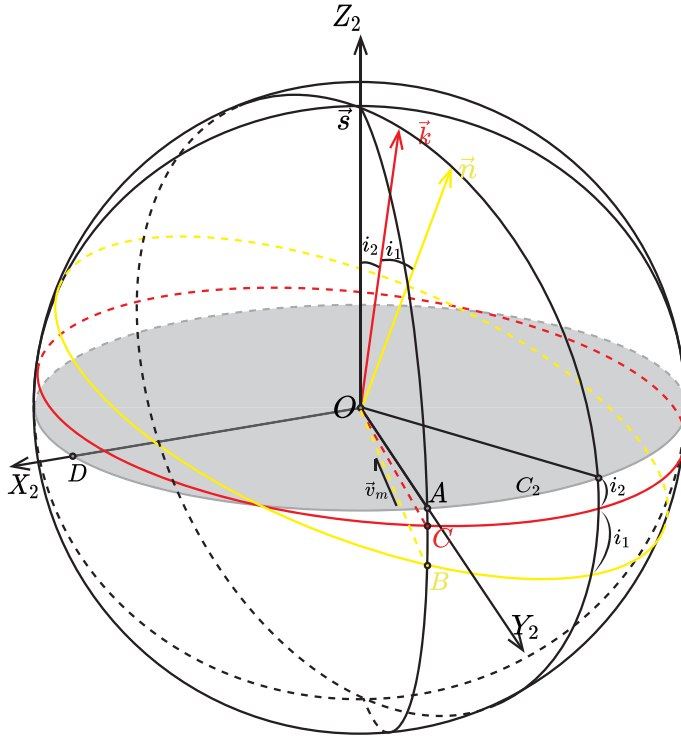


Fig. 6: Sketch for our model in the lunar fixed coordinate system $OX_2Y_2Z_2$. The origin O is at the center of the Moon. The Z_2 -axis is parallel to the lunar spin axis \vec{s} and the X_2 -axis points to the mean sub earth point. \vec{k} is the ecliptic normal. \vec{n} is the lunar orbit normal. Point A, B, and C are on the intersection of the lunar surface and the plane OY_2Z_2 . \overline{OB} is parallel to \vec{v}_m and perpendicular to \vec{n} . Point A is on the lunar equator plane C_2 and it is the ant-apex point ($90^\circ E, 0^\circ N$). Point C is on the ecliptic plane. Point D is the mean sub-earth point.

planets and moons, especially for the types of spin-orbit resonance. For example, Mercury is tidally locked with the Sun in a 3:2 resonance. The cratering rate distribution of 3:2 Resonance is detailed in the Figure 7 Figure 7(a) shows the distribution of cratering rate for 3:2 resonance. This cratering rate asymmetry has been reported in Wieczorek et al. (2012). They predict the cratering asymmetry maximizes at ($0^\circ E, 0^\circ N$) and ($180^\circ E, 0^\circ N$) and minimizes at ($\pm 90^\circ E, 0^\circ N$). Both of this study and Wieczorek et al. (2012) predict the distance between maxima of cratering asymmetry is 180° . The difference between this study and Wieczorek et al. (2012) may be from the ignorance of the non-uniformity on the azimuth of asteroids velocity in this study and different definition of prime meridian between this study and Wieczorek et al. (2012). In Figure 7(b), the cratering with orbital eccentric $e = 0$ shows a different distribution from $e = 0.205$ for 3:2 resonance. The longitudinal variation of cratering rate is diminished by rotation of planets and moons with eccentric $e = 0$. However, in the cratering rate on the Moon, the difference caused by eccentric is less than 0.2%. The influences of eccentric is probably related to the types of spin-orbit resonance and will be investigated in a future work.

5 CONCLUSION

In this study, we have presented an extension of Wang & Zhou (2016) and Le Feuvre & Wieczorek (2011) to calculate the lunar cratering asymmetry with high obliquity and inclination. Different from previous

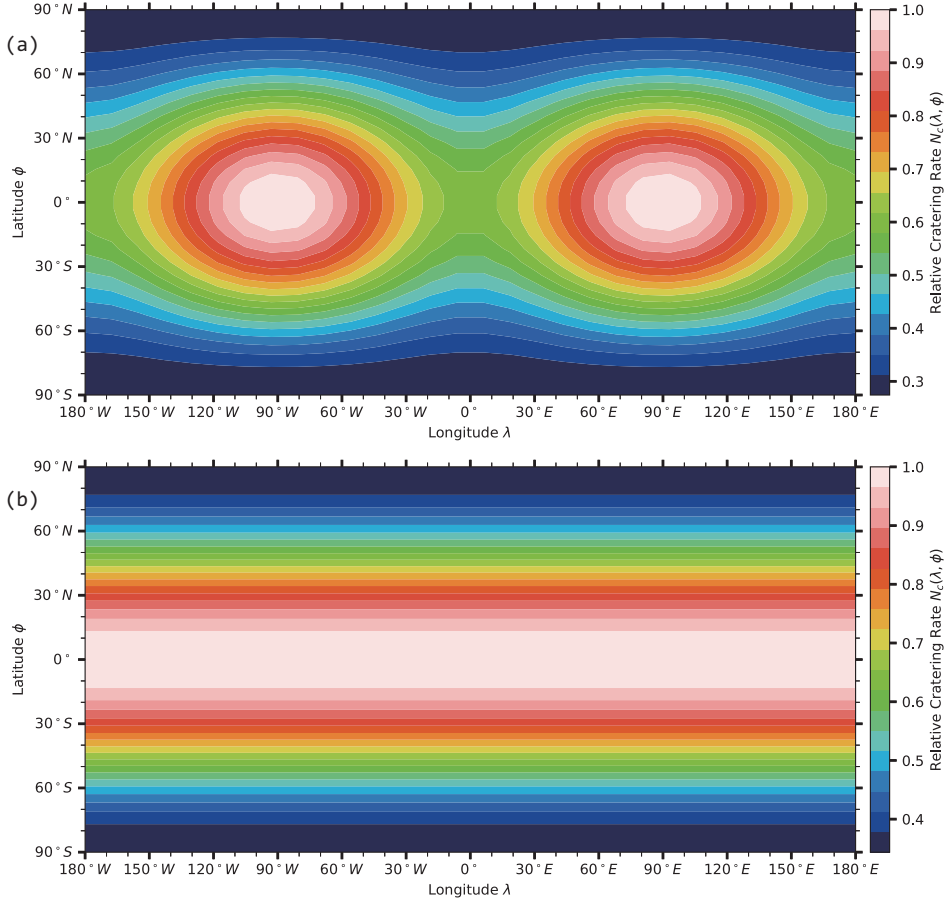


Fig. 7: The relative cratering rate for 3:2 resonance. The maximum is set to 1.00. longitudes 0° and 180° are subsolar points when $M = 0$. In subfigure (a), the orbital eccentric is 0.205. In subfigure (b), the orbital eccentric is 0.0.

models, this model is also able to calculate the cratering asymmetry with different Cassini states, and synchronous rotating speed. This model gives consistent results with previous with low obliquity and inclination. When the obliquity, inclination and Earth-Moon distance are at current values, this model gives an cratering asymmetry maximizing at $(90^\circ W, 0^\circ N)$ and minimizing at $(90^\circ E, \pm 53^\circ N)$ using the encountering velocity inclination distribution calculated in Le Feuvre & Wieczorek (2008). The apex/ant-apex ratio of this asymmetry is 1.36 and the pole/equator ratio is 0.87. In order to calculate the cratering rate with high obliquity and inclination, we have assumed the orbital obliquity and inclination of the Moon don't affect the asteroids population encountering with the Moon. Increasing the orbital obliquity and inclination of the Moon reduces the apex/ant-apex ratio. According to the evolution of orbital obliquity and inclination of the Moon, this model gives an increasing trend in apex/ant-apex ratio with the Earth-Moon distance between $[35R_e, 42R_e]$. This ratio was predicted decreased with the increasing of Earth-Moon distance in previous studies. Besides the cratering rate, this model also gives the spatial variation of impact flux and impact normal speed. Our results provide the quantitative information for evaluating and rectifying the lunar cratering chronology.

Acknowledgements We thank M. A. Wieczorek and W. Fa for instructive discussion at the early stage of this study. We also thank J.-L. Zhou for constructive and insightful suggestions on our research focus. We thank careful reviews by two anonymous reviewers. Computations were conducted on the High-performance Computing Platform of Peking University and the Pawsey Supercomputing Centre with funding from the Australian Government and the Government of Western Australia. Z.Y. is supported by the B-type Strategic Priority Program of the Chinese Academy of Sciences, Grant No. XDB41000000 and NSFC 41972321. N.Z. is grateful for NSFC 41674098, CNSA D020205 and the B-type Strategic Priority Program of the Chinese Academy of Sciences, Grant No. XDB18010104. This research has made use of data and/or services provided by the International Astronomical Union's Minor Planet Center.

References

- Bandermann, L. W., & Singer, S. F. 1973, *Icarus*, 19, 108
- Bottke, W. F., Morbidelli, A., Jedicke, R., et al. 2002, *Icarus*, 156, 399
- Colombo, G. 1965, *Nature*, 208, 575
- Fassett, C. I., Head, J. W., Kadish, S. J., et al. 2012, *Journal of Geophysical Research: Planets*, 117
- Gallant, J., Gladman, B., & Čuk, M. 2009, *Icarus*, 202, 371
- Greenberg, R. 1982, *The Astronomical Journal*, 87, 184
- GSFC. 2008, LRO Project White Paper Version, 4, 1
- Hartmann, W. K. 1970, *Icarus*, 13, 299
- Hartmann, W. K., & Neukum, G. 2001, *Space Science Reviews*, 96, 165
- Hiesinger, H., Jaumann, R., Neukum, G., & Head, J. W. 2000, *Journal of Geophysical Research*, 105, 29239
- Holsapple, K. A., & Housen, K. R. 2007, *Icarus*, 191, 586
- Horedt, G. P., & Neukum, G. 1984, *Icarus*, 60, 710
- Korycansky, D. G., & Zahnle, K. J. 2005, *Planetary and Space Science*, 53, 695
- Le Feuvre, M., & Wieczorek, M. A. 2008, *Icarus*, 197, 291
- Le Feuvre, M., & Wieczorek, M. A. 2011, *Icarus*, 214, 1
- McGill, G. E. 1977, *Geological Society of America Bulletin*, 88, 1102
- Neukum, G. 1984, *Meteorite bombardment and dating of planetary surfaces*, PhD thesis, National Aeronautics and Space Administration, Washington, DC.
- Neukum, G., Ivanov, B. A., & Hartmann, W. K. 2001a, *Space Science Reviews*, 96, 55
- Neukum, G., König, B., & Arkani-Hamed, J. 1975, *The moon*, 12, 201
- Neukum, G., Oberst, J., Hoffmann, H., Wagner, R., & Ivanov, B. A. 2001b, *Planetary and Space Science*, 49, 1507
- Opik, E. J. 1951, *Proc. R. Irish Acad. Sect. A*, 54, 165
- Strom, R. G., Malhotra, R., Xiao, Z.-Y., et al. 2015, *Research in Astronomy and Astrophysics*, 15, 407
- Wang, N., & Zhou, J. L. 2016, *Astronomy & Astrophysics*, 594
- Ward, W. R. 1975, *Science*, 189, 377
- Wetherill, G. W. 1967, *Journal of Geophysical Research (1896-1977)*, 72, 2429

Wieczorek, M. A., Correia, A. C. M., Le Feuvre, M., Laskar, J., & Rambaux, N. 2012, *Nature Geoscience*, 5, 18

Wiesel, W. 1971, *Icarus*, 15, 373

Zahnle, K., Schenk, P., Sobieszczyk, S., Dones, L., & Levison, H. F. 2001, *Icarus*, 153, 111

Ćuk, M., & Burns, J. A. 2004, *The Astronomical Journal*, 128, 2518

Ćuk, M., Hamilton, D. P., Lock, S. J., & Stewart, S. T. 2016, *Nature*, 539, 402

Appendix A: ASTEROIDS ENCOUNTERING WITH THE MOON WITH HIGH OBLIQUITY AND INCLINATION

In section 2.1, we assumed the concentration of asteroids encountering with the Moon is unaffected by the orbital obliquity and inclination of the Moon. Although the probability of asteroids encountering with the Moon has been estimated based on (Opik 1951; Wetherill 1967; Greenberg 1982) and it has been demonstrated the probability encountering with the Moon is similar with the Earth when the lunar inclination and obliquity is about 0 in Figure 6 of Le Feuvre & Wieczorek (2008). But when the inclination and obliquity is high, the rationality of our assumption is uncertain. In this section we introduce a different framework to prove this assumption. For any asteroid with semi-major axis, eccentricity, inclination, longitude of ascending node, argument of perihelion, true anomaly, mean anomaly and eccentric anomaly are $(a, e, i, \Omega, \omega, f, M, E)$. Here we use subscript e to represent the orbit of Earth and m to represent the Moon. In the heliocentric ecliptic coordinates system, the position of this asteroid is

$$\vec{r} = rR_z(\Omega)R_x(i)R_z(\omega + f)[1, 0, 0]^T \quad (\text{A.1})$$

$$r = a(1 - e^2)/(1 + e \cos f) = a(1 - e \cos E) \quad (\text{A.2})$$

$$r_{max} = a(1 + e), \quad r_{min} = a(1 - e)$$

For elliptic trajectory,

$$M = E - e \sin E \quad (\text{A.3})$$

$$\cos f = \frac{\cos E - e}{1 - e \cos E} \quad (\text{A.4})$$

$$\sin f = \frac{\sqrt{1 - e^2} \sin E}{1 - e \cos E} \quad (\text{A.5})$$

Using the common assumption: uniform precession of Ω and ω (Opik 1951; Wetherill 1967; Greenberg 1982), for given (a, e, i) the joint probability density is

$$P_{\Omega, \omega, M}(\Omega, \omega, M|a, e, i) = \left(\frac{1}{2\pi}\right)^3 \quad (\text{A.6})$$

$$\begin{aligned} &P_{\Omega, \omega, E}(\Omega, \omega, E|a, e, i) \\ &= P_{\Omega, \omega, M}(\Omega, \omega, M|a, e, i) \left| \frac{\partial M}{\partial E} \right| = \left(\frac{1}{2\pi}\right)^3 (1 + e \sin E) \end{aligned} \quad (\text{A.7})$$

$$\Omega \in [-\pi, \pi], \quad \omega \in [-\pi, \pi], \quad M \in [-\pi, \pi], \quad E \in [-\pi, \pi] \quad (\text{A.8})$$

The position of this asteroid can also be expressed as $\vec{r} = [x, y, z]^T$, then we obtain a transformation: $(\Omega, \omega, E) \mapsto (x, y, z)$.

$$\begin{cases} x = r(\cos \Omega \cos(\omega + f) - \sin \Omega \sin(\omega + f) \cos i) \\ y = r(\sin \Omega \cos(\omega + f) + \cos \Omega \sin(\omega + f) \cos i) \\ z = r \sin(\omega + f) \sin i \end{cases} \quad (\text{A.9})$$

Eq. (A.9) has 4 solutions: $(\Omega_k, \omega_k, E_k), k = 1, 2, 3, 4$.

$$\begin{cases} \cos f_k = \frac{a(1-e^2)}{e\sqrt{x^2+y^2+z^2}} - \frac{1}{e} \\ \sin(\omega_k + f_k) = \frac{z}{\sqrt{x^2+y^2+z^2} \sin i} \\ \Omega_k = \text{atan2}\left(x \cos(\omega_k + f_k) + y \sin(\omega_k + f_k) \cos i, \right. \\ \quad \left. y \cos(\omega_k + f_k) - x \sin(\omega_k + f_k) \cos i\right) \\ E_k = \text{atan2}\left(\sqrt{x^2+y^2+z^2} \cos f_k + ae, \right. \\ \quad \left. \sqrt{x^2+y^2+z^2} \sin f_k \frac{1}{\sqrt{1-e^2}}\right) \end{cases} \quad (\text{A.10})$$

Using Eqs. (A.6-A.10), the joint probability density is

$$\begin{aligned} P_{x,y,z}(x, y, z|a, e, i) &= \sum_{k=1}^4 \left\| \frac{\partial(\Omega_k, \omega_k, E_k)}{\partial(x, y, z)} \right\| P_{\Omega, \omega, E}(\Omega_k, \omega_k, E_k|a, e, i) \\ &= \frac{1}{2a\pi^3} \frac{1}{\sqrt{r^2 \sin^2 i - z^2}} \frac{1}{\sqrt{(r - r_{min})(r_{max} - r)}}, \quad r = \sqrt{x^2 + y^2 + z^2} \end{aligned} \quad (\text{A.11})$$

In Eq. (A.11), $\frac{\partial(\Omega_k, \omega_k, E_k)}{\partial(x, y, z)}$ is the Jacobi matrix. Eq. (A.11) is valid when $(x, y, z) \in \mathbf{D} = \{|z| \leq |\sin i| r \text{ and } r_{min} \leq r \leq r_{max}\}$. When $(x, y, z) \notin \mathbf{D}$, $P_{x,y,z}(x, y, z|a, e, i) = 0$. This asteroid encountering with a fix point $\vec{r}_0 = [x_0, y_0, z_0]^T$ is defined as $|\vec{r} - \vec{r}_0| \leq \tau$ (τ is different for the Moon and the Earth) and $\tau \ll \min\{|\vec{r}|, |\vec{r}_0|\}$. Then we obtain the probability encountering with a fixed point P_1 and its error δP_1 .

$$\begin{aligned} P_1 &= \iiint_{|\vec{r} - \vec{r}_0| \leq \tau} P_{x,y,z}(x, y, z|a, e, i) dx dy dz \\ &\approx \frac{4}{3} \pi \tau^3 P_{x,y,z}(x_0, y_0, z_0|a, e, i) \end{aligned} \quad (\text{A.12})$$

$$\begin{aligned} \delta P_1 &\approx \iiint_{|\vec{r} - \vec{r}_0| \leq \tau} |\vec{r} - \vec{r}_0| |\nabla P_{x,y,z}(x_0, y_0, z_0|a, e, i)| dx dy dz \\ &= \pi \tau^4 |\nabla P_{x,y,z}(x_0, y_0, z_0|a, e, i)| \end{aligned} \quad (\text{A.13})$$

Because $P_{x,y,z}$ is not bounded with $(r^2 \sin^2 i - z^2)(r - r_{max})(r - r_{min}) = 0$. Eq.(A.12) and Eq. (A.13) are valid when $\min\{|r \sin i \pm z|, |r - r_{max}|, |r - r_{min}|\} \geq \varepsilon a$ ($\varepsilon > 0$). When $\min\{|r \sin i \pm z|, |r - r_{max}|, |r - r_{min}|\} < \varepsilon a$, the supremum of P_1 can be estimated in spherical coordinates,

$$\begin{aligned} P_1 &\leq \iiint_E P_{x,y,z} r^2 |\sin \theta| dr d\theta d\varphi = \frac{1}{2a\pi^3} \left(\int_{\varphi} d\varphi \right) \\ &\cdot \text{Re} \left(\int_{\theta} \frac{\sin \theta d\theta}{\sqrt{\sin^2 i - \cos^2 \theta}} \right) \text{Re} \left(\int_r \frac{r dr}{\sqrt{(r - r_{min})(r_{max} - r)}} \right) \end{aligned} \quad (\text{A.14})$$

$$E = \left\{ |r - r_0| \leq \tau, |\theta - \theta_0| \leq \arctan \tau / r_0, |\varphi - \varphi_0| \leq \arctan \frac{\tau}{r_0 \cos \theta_0} \right\} \quad (\text{A.15})$$

This section is only a qualitative explanation. For simplicity, following derivations are under the condition: $\min\{|r \sin i \pm z|, |r - r_{max}|, |r - r_{min}|\} \geq \varepsilon a$. When \vec{r}_0 is not fixed, for the Earth $\vec{r}_0 = \vec{r}_e = r_e R_z(\Omega_e) R_x(i_e) R_z(\omega_e + f_e) [1, 0, 0]^T$, this asteroid encounters with the Earth by probability P_2 .

$$\begin{aligned} P_2 &= \iiint_{(\Omega_e, \omega_e, M_e)} P(\Omega_e, \omega_e, M_e | a_e, e_e, i_e) P_1 d\Omega_e d\omega_e dM_e \\ &= 2\pi \iint_{(\omega_e, M_e)} P(\Omega_e = 0, \omega_e, M_e | a_e, e_e, i_e) P_1 d\omega_e dM_e \end{aligned} \quad (\text{A.16})$$

$$\delta P_2 = 2\pi \iint_{(\omega_e, M_e)} P(\Omega_e = 0, \omega_e, M_e | a_e, e_e, i_e) \delta P_1 d\omega_e dM_e \quad (\text{A.17})$$

Eq. (A.16) and Eq. (A.17) use the rotational symmetry about the z axis of $P_{x,y,z}$. For the Moon $\vec{r}_0 = \vec{r}_e + \vec{r}_m = r_e R_z(\Omega_e) R_x(i_e) R_z(\omega_e + f_e) [1, 0, 0]^T + r_m R_z(\Omega_m) R_x(i_m) R_z(\omega_m + f_m) [1, 0, 0]^T$, this asteroid encounters with the Moon by P_3 .

$$\begin{aligned} P_3 &= 2\pi \iint_{(\omega_e, M_e)} P(\Omega_e = 0, \omega_e, M_e | a_e, e_e, i_e) \\ &\quad \iiint_{(\Omega_m, \omega_m, M_m)} P(\Omega_m, \omega_m, M_m | a_m, e_m, i_m) P_1 d\omega_e dM_e d\Omega_m d\omega_m dM_m \end{aligned} \quad (\text{A.18})$$

$$\begin{aligned} \delta P_3 &= 2\pi \iint_{(\omega_e, M_e)} P(\Omega_e = 0, \omega_e, M_e | a_e, e_e, i_e) \\ &\quad \iiint_{(\Omega_m, \omega_m, M_m)} P(\Omega_m, \omega_m, M_m | a_m, e_m, i_m) \delta P_1 d\omega_e dM_e d\Omega_m d\omega_m dM_m \end{aligned} \quad (\text{A.19})$$

The difference between P_2 and P_3 can be estimated by

$$\begin{aligned} |P_2 \tau_e^{-3} - P_3 \tau_m^{-3}| &\leq 2\pi \iint_{(\omega_e, M_e)} P(\Omega_e = 0, \omega_e, M_e | a_e, e_e, i_e) \iiint_{(\Omega_m, \omega_m, M_m)} P(\Omega_m, \omega_m, M_m | a_m, e_m, i_m) \\ &\quad \times \frac{4\pi}{3} |P_{x,y,z}(x_m + x_e, y_m + y_e, z_m + z_e | a, e, i) - P_{x,y,z}(x_e, y_e, z_e | a, e, i)| d\omega_e dM_e d\Omega_m d\omega_m dM_m \end{aligned} \quad (\text{A.20})$$

From Eq. (A.20), P_3 can be estimated by $P_2 \frac{\tau_m^3}{\tau_e^3}$. While $P_2 \frac{\tau_m^3}{\tau_e^3}$ is independent of lunar inclination and obliquity, therefore we can use the concentration of asteroids encountering with the Moon with low inclination and obliquity to replace the concentration with high inclination and obliquity. We note that when $(a_e, i_e, e_e) = (1, 0, 0)$, for 87% of the near-earth orbits (the dataset of near-earth orbits is taken from the International Astronomical Union's website), the relative error between $P_2 \frac{\tau_m^3}{\tau_e^3}$ and P_3 calculated by Eq. (A.20) is less than 5%.